Inorg. Chem. **2009**, *48*, 287−295

Guest Inclusion and Interpenetration Tuning of Cd(II)/Mn(II) Coordination Grid Networks Assembled from a Rigid Linear Diimidazole Schiff Base Ligand

Qing Wang,[†] Jianyong Zhang,*[,†] Chun-Feng Zhuang,[†] Yu Tang,[‡] and Cheng-Yong Su*[,†]

MOE Laboratory of Bioinorganic and Synthetic Chemistry, State Key Laboratory of Optoelectronic Materials and Technologies, School of Chemistry and Chemical Engineering, Sun Yat-Sen University, Guangzhou 510275, China, and State Key Laboratory of Applied Organic Chemistry, Lanzhou University, Lanzhou 730000, China

Received September 16, 2008

Cd(II)/Mn(II) coordination grid networks containing large meshes have been assembled from a long rigid ligand, 2,5-bis(4′-(imidazol-1-yl)benzyl)-3,4-diaza-2,4-hexadiene (ImBNN), and $M(CF_3SO_3)_2$ (M = Cd and Mn) salts, and their interpenetration change upon guest inclusion has been investigated with a series of aromatic molecules. Without guest molecules, the grid networks are triply interpenetrated to form closely packed layer structures $[M(ImBNN)_2(CF_3SO_3)_2]_n$ (M = Cd (**1**) and Mn (**2**)), but when guest molecules are introduced, the triply interpenetrated frameworks are changed to doubly interpenetrated ones with the inclusion of various aromatic molecules, namely, $\{[M(ImBNN)_2(CF_3SO_3)_2]\supset guest\}_n$ (M = Cd, guest = *o*-xylene (**3**), naphthalene (**4**), phenanthrene (**5**), and pyrene (**6**); M = Mn, guest = benzene (**7**), *p*-xylene (**8**), naphthalene (**9**), phenanthrene (**10**), and pyrene (**11**)). These complexes have been characterized by means of single-crystal X-ray diffraction, X-ray powder diffraction, and IR spectra. The guest-inclusion/desorption behaviors of representative complexes have been studied by thermogravimetric analyses and ^1H NMR measurements. The grid networks display strong preference for aromatic guest inclusion, but less selectivity toward shape and size difference. Tuning of network interpenetration from 3-fold to 2-fold has been successfully achieved through the introduction of guest molecules, when the network displays flexibility to change cavity size to match the guest molecules.

Introduction

Coordination polymers (CPs) have attracted great attention due to their potential applications in gas sorption,[1] enantioselective separation,[2] catalysis,[3] anion/guest exchange,[4] magnetism,[5] and so forth. CPs are also of interest due to their stimuli responsive property. For example, the framework can change to fit specific guest molecules upon guest uptake. In an effort to explore gas/guest storage properties, chemists have designed various rigid ligands to synthesize coordination frameworks with permanent porosity.[6,7] One of the efforts is to prepare long bridging ligands which are expected to create larger cavity sizes; however, simultaneous interpenetration of the networks often occurs along self-assembly.[8] Nevertheless, although mutual interpenetration of the networks usually fills up potential cavities and reduces porosity, excellent gas adsorption capacity has been proven possible for the interpenetrated coordination networks.[9] Moreover, the interpenetration may be able to sustain a framework showing dynamic porosity. For instance, the cavity inside an interpenetrated coordination polymer can change along sliding between the individual networks. The sliding of 2D networks and clathration could be triggered by guest exchange/inclusion, resulting in changes in the dimensions of channels.[10] There are also a few reports that interpenetrated networks could shrink and swell to show some flexible properties when guest molecules are removed and then readsobed.[11] Therefore, the construction of CPs containing large pores, which allows multiple interpenetrations on one hand and makes it possible to tune interpenetration responsive to host−guest interactionon on the other hand, becomes a promising approach to obtaining functional or "smart" materials.

* Authors to whom correspondence should be addressed. E-mail: zhjyong@mail.sysu.edu.cn (J.Z.), cesscy@mail.sysu.edu.cn (C.-Y.S.).
† Sun Yat-Sen University.
‡ Lanzhou University.

10.1021/ic801770n CCC: $40.75
Published on Web 11/26/2008

A number of methods are known from the literature to be able to prevent or reduce the interpenetration of CPs, such as the preparation of charged networks, introduction of strong interactions between the networks, clathration of guest molecules, utilization of large building blocks, and design of an inherently porous network topology.[12] Among these methods, clathration of guest molecules is of particular interest. Proper choice of suitable guests can not only transform a higher interpenetrated CP to a lower interpenetrated one but may also play an important role in the dynamics of the framework.[13] We have previously reported

Scheme 1. The Ligand ImBNN in trans-*Z* Configuration

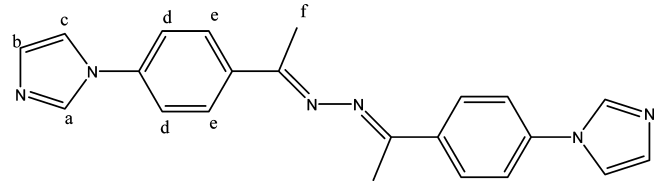

noninterpenetrated square-grid coordination polymers based on a long rigid N,N′-type ligand, 2,5-bis(4′-(imidazol-1-yl)benzyl)-3,4-diaza-2,4-hexadiene (ImBNN; Scheme 1), and found that both the channel-containing structure and the nonporous structure could be formed by altering the solvent systems.[14] Herein, we report the assembly of interpenetration-adjustable Cd(II)/Mn(II) grid coordination networks of the ImBNN ligand. Tuning of 3-fold interpenetrated two-dimensional (2D) networks to 2-fold interpenetrated ones has been studied with a series of aromatic guest molecules. The thermostability and guest adsorption/desorption behaviors have also been investigated by thermogravimetric analysis and power X-ray diffraction (XRD).

Result and Discussion

Syntheses and Crystal Structures. The ligand ImBNN was synthesized following the literature method by the reaction of hydrazine with 4-(imidazol-1-yl)acetophenone.[14] The Cd(II) complexes $[Cd(ImBNN)_2(CF_3SO_3)_2]_n$ (**1**) and $\{[Cd(ImBNN)_2(CF_3SO_3)_2]\supset guest\}_n$ (**3**−**6**) were prepared by the reaction of $Cd(CF_3SO_3)_2 \cdot 6H_2O$ with ImBNN in the absence or presence of guest molecules, respectively (Figure 1). In general, the solution of the metal salt was carefully layered onto the mixed solutions of the ligand and guests (no guest for **1**, guest *o*-xylene for **3**, naphthalene for **4**, phenanthrene for **5**, and pyrene for **6**). The Mn(II) analogues, $[Mn(ImBNN)_2(CF_3SO_3)_2]_n$ (**2**) and $\{[Mn(ImBNN)_2(CF_3SO_3)_2]\supset guest\}_n$ (**7**−**11**) were prepared by the reaction of $Mn(CF_3SO_3)_2$ with ImBNN by diffusing Et_2O into the guest-free/-containing reaction mixtures (no guest for **2**, guest benzene for **7**, *p*-xylene for **8**, naphthalene for **9**, phenanthrene for **10**, and pyrene for **11**). The target crystalline

(1) (a) Noro, S.-i.; Kitagawa, S.; Kondo, M.; Seki, K. *Angew. Chem., Int. Ed.* **2000**, *39*, 2081–2084. (b) Seki, K. *Chem. Commun.* **2001**, 1496–1497. (c) Eddaoudi, M.; Kim, J.; Rosi, N.; Vodak, D.; Wachter, J.; O'Keeffe, M.; Yaghi, O. M. *Science* **2002**, *295*, 469–472. (d) Li, D.; Kaneko, K. *J. Phys. Chem. B* **2000**, *104*, 8940–8945. (e) Chui, S. S.-Y.; Lo, S. M.-F.; Charmant, J. P. H.; Orpen, A. G.; Williams, I. D. *Science* **1999**, *283*, 1148–1150. (f) Barthelet, K.; Marrot, J.; Riou, D.; Férey, G. *Angew. Chem., Int. Ed.* **2002**, *41*, 281–284. (g) Chen, C.-L.; Kang, B.-S.; Su, C.-Y. *Aust. J. Chem.* **2006**, *59*, 3–18.

(2) (a) Seo, J. S.; Wand, D.; Lee, H.; Jun, S. I.; Oh, J.; Jeon, Y.; Kim, K. *Nature* **2000**, *404*, 982–986. (b) Li, G.; Yu, W.; Ni, J.; Liu, T.; Liu, Y.; Sheng, E.; Cui, Y. *Angew. Chem., Int. Ed.* **2008**, *47*, 1245–1249. (c) Evans, O. R.; Ngo, H. L.; Lin, W. *J. Am. Chem. Soc.* **2001**, *123*, 10395–10396.

(3) (a) Fujita, M.; Kwon, Y. J.; Washizu, S.; Ogura, K. *J. Am. Chem. Soc.* **1994**, *116*, 1151–1152. (b) Sawaki, T.; Dewa, T.; Aoyama, Y. *J. Am. Chem. Soc.* **1998**, *120*, 8539–8640. (c) Sawaki, T.; Aoyama, Y. *J. Am. Chem. Soc.* **1999**, *121*, 4793–4798. (d) Pan, L.; Liu, H.; Lei, X.; Huang, X.; Olson, D. H.; Turro, N. J.; Li, J. *Angew. Chem., Int. Ed.* **2003**, *42*, 542–546.

(4) (a) Hoskins, B. F.; Robson, R. *J. Am. Chem. Soc.* **1990**, *112*, 1546–1554. (b) Lee, E.; Kim, J.; Heo, J.; Whang, D.; Kim, K. *Angew. Chem., Int. Ed.* **2001**, *40*, 399–402. (c) Yaghi, O. M.; Li, H. *J. Am. Chem. Soc.* **1995**, *117*, 10401–10402. (d) Hamilton, B. H.; Kelly, K. A.; Wagler, T. A.; Espe, M. P.; Ziegler, C. J. *Inorg. Chem.* **2002**, *41*, 4984–4986. (e) Jung, O.-S.; Kim, Y. J.; Kim, K. M.; Lee, Y.-A. *J. Am. Chem. Soc.* **2002**, *124*, 7906–7907. (f) Min, K. S.; Suh, M. P. *J. Am. Chem. Soc.* **2000**, *122*, 6834–6840. (g) Jung, O.-S.; Kim, Y. J.; Lee, Y.-A.; Yoo, K. H. *Chem. Lett.* **2002**, 500–501. (h) Pan, L.; Woodlock, E. B.; Wang, X.; Lam, K.-C.; Rheingold, A. L. *Chem. Commun.* **2001**, 1762–1763. (i) Jung, O.-S.; Kim, Y. J.; Lee, Y.-A.; Park, J. K.; Chae, H. K. *J. Am. Chem. Soc.* **2000**, *122*, 9921–9925.

(5) (a) Halder, G. J.; Kepert, C. J.; Moubaraki, B.; Murray, K. S.; Cashion, J. D. *Science* **2002**, *298*, 1762–1765. (b) Wang, Z.; Zhang, B.; Fujiwara, H.; Kobayashi, H.; Kurmoo, M. *Chem. Commun.* **2004**, 416–417. (c) Bourne, S. A.; Lu, J.; Mondal, A.; Moulton, B.; Zaworotko, M. J. *Angew. Chem., Int. Ed.* **2001**, *40*, 2111–2113.

(6) (a) Rosseinsky, M. J. *Microporous Mesoporous Mater.* **2004**, *73*, 15–30. (b) Kitagawa, S.; Kitaura, R.; Noro, S.-I. *Angew. Chem., Int. Ed.* **2004**, *43*, 2334–2375. (c) Kepert, C. J. *Chem. Commun.* **2006**, 695–700.

(7) (a) Eddaoudi, M.; Moler, D. B.; Li, H.-L.; Chen, B.-L.; Reineke, T. M.; O'Keeffe, M.; Yaghi, O. M. *Acc. Chem. Res.* **2001**, *34*, 319–330. (b) Janiak, C. *Dalton Trans.* **2003**, 2781–2804. (c) Takamizawa, S.; Nakata, E.-I.; Akatsuka, T. *Angew. Chem., Int. Ed.* **2006**, *45*, 2216–2221. (d) Bradshaw, D.; Warren, J. E.; Rosseinsky, M. J. *Science* **2007**, *315*, 977–980. (e) Halder, G. J.; Kepert, C. J. *Aust. J. Chem.* **2006**, *59*, 597–604. (f) Suh, M. P.; Cheon, Y. E. *Aust. J. Chem.* **2006**, *59*, 605–612. (g) Vittal, J. J. *Coord. Chem. Rev.* **2007**, *251*, 1781–1795. (h) Mulfort, K. L.; Hupp, J. T. *J. Am. Chem. Soc.* **2007**, *129*, 9604–9605. (i) Kerckhoffs, J. M. C. A.; Peberdy, J. C.; Meistermann, I.; Childs, L. J.; Isaac, C. J.; Pearmund, C. R.; Reudegger, V.; Khalid, S.; Alcock, N. W.; Hannon, M. J.; Rodger, A. *Dalton Trans.* **2007**, 734–742. (j) Khlobystov, A. N.; Champness, N. R.; Roberts, C. J.; Tendler, S. J. B.; Thompson, C.; Schröder, M. *CrystEngComm* **2002**, *4*, 426–431. (k) Su, C.-Y.; Goforth, A. M.; Smith, M. D.; Pellechia, P. J.; zur Loye, H.-C. *J. Am. Chem. Soc.* **2004**, *126*, 3576–3586.

(8) Batten, S. R.; Robson, R. *Angew. Chem., Int. Ed.* **1998**, *41*, 1460–1494.

(9) (a) Rowsell, J. L. C.; Yaghi, O. M. *Angew. Chem., Int. Ed.* **2005**, *44*, 4670. (b) Kesanli, B.; Cui, Y.; Smith, M. R.; Bittner, E. W.; Bockrath, B. C.; Lin, W. *Angew. Chem., Int. Ed.* **2005**, *44*, 72. (c) Chen, B.; Ma, S.; Zapata, F.; Lobkovsky, E. B.; Yang, J. *Inorg. Chem.* **2006**, *45*, 5718.

(10) (a) Biradha, K.; Hongo, Y.; Fujita, M. *Angew. Chem., Int. Ed.* **2002**, *41*, 3395–3398. (b) Takamizawa, S.; Nakata, E.-I.; Yokoyama, H.; Mochizuki, K.; Mori, W. *Angew. Chem., Int. Ed.* **2003**, *42*, 4331–4334. (c) Suh, M. P.; Ko, J. W.; Choi, H. J. *J. Am. Chem. Soc.* **2002**, *124*, 10976–10977. (d) Kondo, A.; Noguchi, H.; Ohnishi, S.; Kajiro, H.; Tohdoh, A.; Hattori, Y.; Xu, W.-C.; Tanaka, H.; Kanoh, H.; Kaneko, K. *Nano. Lett* **2006**, *6*, 2581–2584.

(11) Biradha, K.; Fujita, M. *Angew. Chem., Int. Ed.* **2002**, *41*, 3392–3395.

(12) (a) James, S. L. *Chem. Soc. Rev.* **2003**, *32*, 276–288. (b) Zheng, S.-R.; Yang, Q.-Y.; Liu, Y.-R.; Zhang, J.-Y.; Tong, Y.-X.; Zhao, C.-Y.; Su, C.-Y. *Chem. Commun.* **2008**, 356–358. (c) Lü, X.-Q.; Jiang, J.-J.; zur Loye, H.-C.; Kang, B.-S.; Su, C.-Y. *Inorg. Chem.* **2005**, *44*, 1810–1817.

(13) (a) Kondo, M.; Irie, Y.; Shimizu, Y.; Miyazawa, M.; Kawaguchi, H.; Nakamura, A.; Naito, T.; Maeda, K.; Uchida, F. *Inorg. Chem.* **2004**, *43*, 6139–6141. (b) KumarMaji, T.; Uemura, K.; Chang, H.-C.; Matsuda, R.; Kitagawa, S. *Angew. Chem.* **2004**, *116*, 3331–3334. (c) Wei, Q.; Nieuwenhuyzen, M.; Meunier, F.; Hardacre, C.; James, S. L. *Dalton Trans.* **2004**, 1807–1811. (d) Uemura, K.; Kitagawa, S.; Fukui, K.-I.; Saito, K. *J. Am. Chem. Soc.* **2004**, *126*, 3817–3828. (e) Biradha, K.; Domasevitch, K. V.; Moulton, B.; Seward, C.; Zaworotko, M. J. *Chem. Commun.* **1999**, 1327–1328.

(14) Chen, C.-L.; Goforth, A. M.; Smith, M. D.; Su, C.-Y.; zur Loye, H.-C. *Inorg. Chem.* **2005**, *44*, 8762–8769.

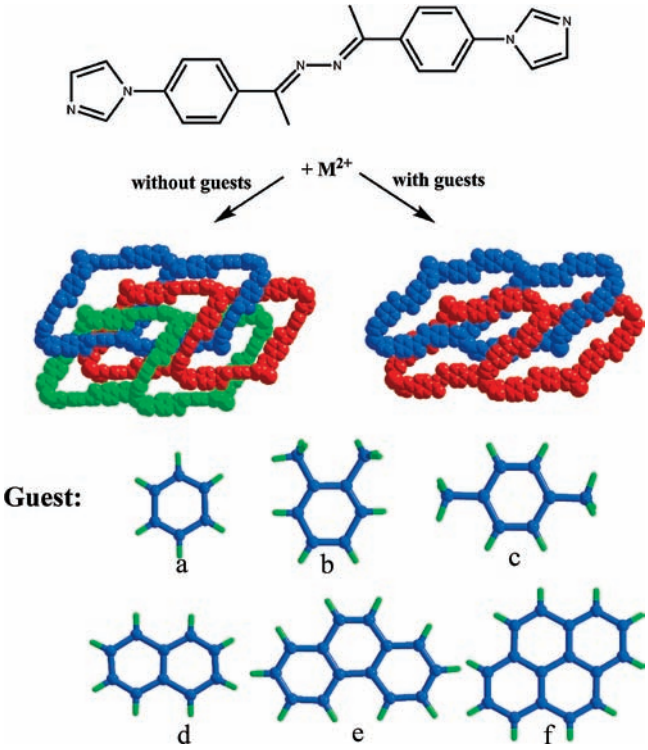

Figure 1. Formation of 3-fold interpenetrated grid networks in the absence of guest molecules, and 2-fold interpenetrated ones in the presence of guests: (a) benzene, (b) *o*-xylene, (c) *p*-xylene, (d) naphthalene, (e) phenanthrene, and (f) pyrene.

Table 1. Assignment of ^{1}H NMR of Complexes **3**−**6** (300 MHz, DMSO-d_6, 25 °C)

	δ/ppm			
assignment	**3**	**4**	**5**	**6**
singlet, 2H, Im-H(H_a)	8.37	8.35	8.38	8.37
doublet, 4H, Ph-H(H_e)	8.07−8.06	8.05−8.03	8.06−8.03	8.08−8.06
	^3J = 8.8	^3J = 8.4	^3J = 8.7	^3J = 7.5
singlet, 2H, Im-H(H_c)	7.86	7.82	7.84	7.87
doublet, 4H, Ph-H(H_d)	7.79−7.77	7.77−7.74	7.74−7.71	7.78−7.75
	^3J = 8.8	^3J = 8.7	^3J = 10.5	^3J = 8.7
singlet, 2H, Im-H(H_b)	7.16	7.14	7.14	7.15
singlet, Me-H(H_f)	2.34	2.33	2.33	2.33
guest	*o*-xylene	naphthalene	phenanthrene	pyrene
	7.13−7.06	7.90−7.88	8.82−8.79	8.29−8.27
	2.21	7.51−7.48	7.98−7.95	8.17
			7.84	8.08
			7.69−7.60	

complexes formed over a period of about two days to two weeks in various guest-free/-containing MeOH/$CHCl_3$ solvent systems. The presence of $CF_3SO_3^-$ in the Cd(II)/Mn(II) complexes **1**−**11** was confirmed by the characteristic IR absorption bands at about 1300 and 1260−1230 cm^{-1}, corresponding to the C−F and S−O vibrations. The presence of guest molecules C_6H_6, C_8H_{10}, $C_{10}H_8$, $C_{14}H_{10}$, and $C_{16}H_{10}$ in complexes **3**−**6** has been verified by ^{1}H NMR spectra (see Table 1).

X-ray single-crystal crystallographic analyses reveal that all of the complexes, **1**−**11**, are characteristic of grid structures of (4, 4) net topology. The ligand ImBNN adopts a trans-*Z* configuration.[14] The center metal ion Cd(II)/Mn(II) adopts an octahedral geometry, and the Cd(II)/Mn(II) ion lying on an inversion center is hexacoordinate with four N-donor atoms from four different ImBNN ligands which occupy the equatorial positions and two O-donor atoms from two $CF_3SO_3^-$ anions which occupy the axial positions (Figure 2a).

The grid size of these (4, 4) networks is determined by a 76-membered M_4L_4 macrocyclic ring, which can be simplified as a rhombus with dimensions estimated by two diagonal M···M distances and two vertex angles ∠M···M···M within the M_4L_4 basic ring (see Table 2). The Cd(II) complex **1** has a size of 35.5 × 23.7 Å, with the angles being 112.5 and 67.6°, and the Mn(II) analogue **2** has a similar size of 35.2 × 23.8 Å, with the angles being 111.8 and 68.2°. Although huge cavities are formed in a single (4, 4) network, no guest/solvent molecules, however, are found in the frameworks of **1** and **2** despite the fact that MeOH/$CHCl_3$ solvents were used in crystallization. Instead, the individual grid networks interweave with each other to result in 3-fold parallel interpenetration, preventing substantial void space so that densely entangled frameworks are formed excluding solvents residing in the crystal lattice. Different from our previously synthesized noninterpenetrated coordination polymers based on the same ligand ImBNN with NO_3^- anions,[14] the present complexes display interpenetration behavior, indicating that the linear $CF_3SO_3^-$ anions play a significant role in directing the network packing compared with the planar NO_3^- anions.

Guest Inclusion and Interpenetration Tuning. In order to decrease interpenetration of the spacious grid networks and to create substantial void space, various guests were added in the reaction systems, as described in the Experimental Section. On the basis of structure **1**, guest inclusion Cd(II) complexes **3**−**6**, $\{[Cd(ImBNN)_2(CF_3SO_3)_2]\supset(guest)_x\}_n$, were obtained by adding *o*-xylene, naphthalene, phenanthrene, and pyrene, respectively, and on the basis of structure **2**, similar guest inclusion Mn(II) complexes **7**−**11**, $\{[Mn(ImBNN)_2(CF_3SO_3)_2]\supset(guest)_x\}_n$, were obtained by adding benzene, *p*-xylene, naphthalene, phenanthrene, and pyrene, respectively. All of these guest inclusion products have been characterized by the method of single-crystal X-ray diffraction analyses. In addition, the powder X-ray diffraction patterns were recorded to check the solid-state phase purity of the bulky samples of complexes **1**−**11** (Figure S2−4, Supporting Information). The pattern of complex **4** shows a few peaks which are absent in the simulated one, indicating that the bulky sample of complex **4** may not be a single phase, probably contaminated by a second phase. For all other complexes, the measured patterns are comparable with the simulated ones, indicative of satisfactory solid-state phase purity.

The X-ray diffraction results confirmed that a series of aromatic molecules of varied shapes and sizes could be clathrated into the grid networks. Comparable with those in **1** and **2**, the coordination networks in complexes **3**−**11** retain the (4, 4) topological net structure (Figure 4) and display the same layered crystal packing (Figure 5 and Figure S1, Supporting Information). However, upon guest inclusion, the structures were changed from 3-fold interpenetration to 2-fold interpenetration. Formation of the

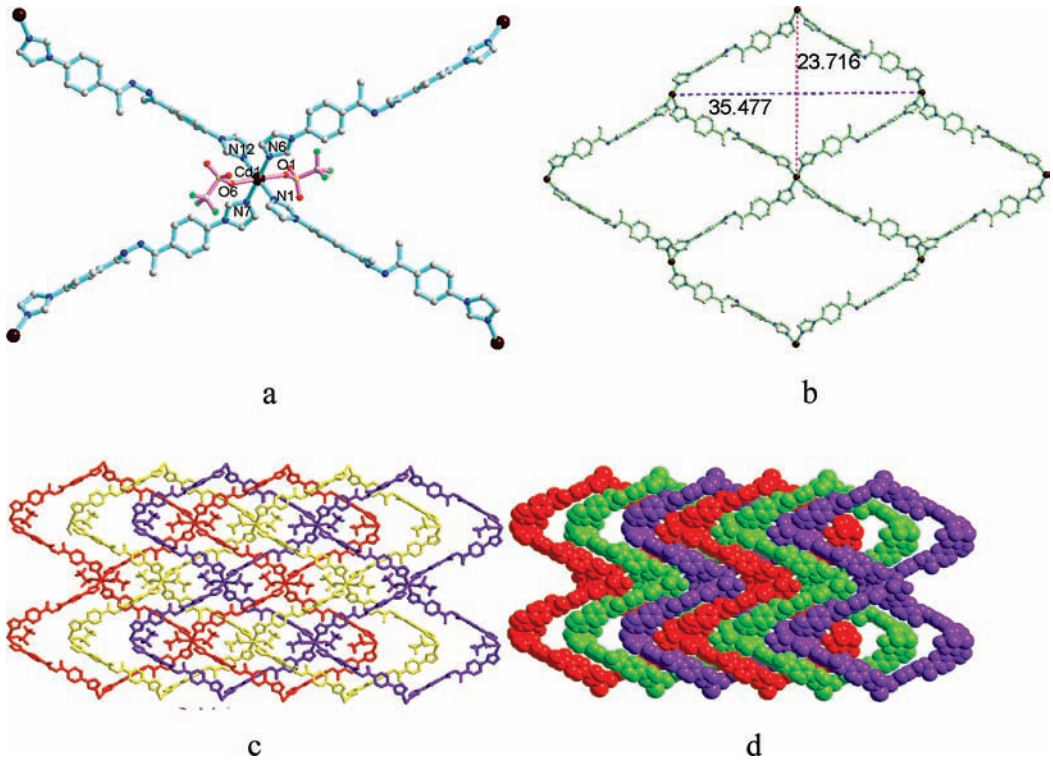

Figure 2. Crystal structure of complex **1**: (a) molecular structure with coordinated atomic labeling scheme, (b) (4, 4) net and M_4L_4 rhombic rings, (c) 3-fold interpenetration of grid networks in stick mode, and (d) 3-fold interpenetration in space-filling mode.

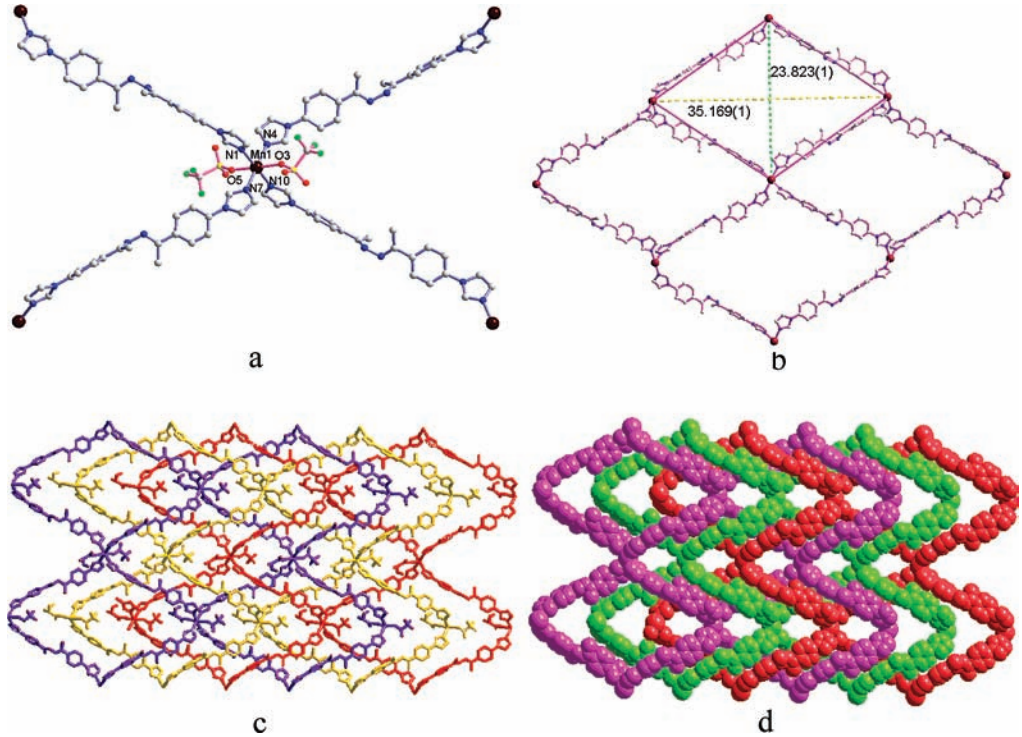

Figure 3. Crystal structure of complex **2**: (a) molecular structure with coordinated atomic labeling scheme, (b) (4, 4) net and M_4L_4 rhombic rings, (c) 3-fold interpenetration of grid networks in stick mode, and (d) 3-fold interpenetration in space-filling mode.

lower-fold interpenetration leads to less dense framework entanglement in comparison to the 3-fold interpenetration, therefore, allowing guest molecules to reside in the cavities formed inside the framework. The number of guest molecules hosted inside the framework depends on their shape and size. When the guests are benzene or *o*-xylene, which are relatively short compared with the cavity size of the host framework, two guest molecules are accommodated per rhombic grid, whereas when the guests are longer (some bigger) such as *p*-xylene, naphthalene,

Table 2. Structural Comparison of **1**−**11**

	M_4L_4						
complex	M···M distance/Å		angle/deg		interpenetration	guest	potential solvent area volume/%
1	35.477	23.712	112.47	67.55	3-fold	none	0
2	35.169	23.823	111.77	68.21	3-fold	none	0.6
3	37.642	20.218	123.47	56.47	2-fold	C_8H_{10}	13.8
4	37.374	20.171	123.51	56.49	2-fold	$C_{10}H_8$	12.0
5	37.544	20.211	123.19	56.81	2-fold	$C_{14}H_{10}$	12.7
6	37.844	20.274	123.71	56.29	2-fold	$C_{16}H_{10}$	13.3
7	37.106	20.434	122.26	57.67	2-fold	C_6H_6	12.7
8	37.217	20.251	122.89	57.11	2-fold	C_8H_{10}	12.2
9	37.163	20.304	122.70	57.30	2-fold	$C_{10}H_8$	12.2
10	37.374	20.211	123.19	56.81	2-fold	$C_{14}H_{10}$	12.6
11	37.384	20.236	123.15	56.85	2-fold	$C_{16}H_{10}$	12.9

phenanthrene, or pyrene, the framework can only host one molecule per grid, as shown in Figure 6.

Tuning of the 3-fold interpenetration to 2-fold interpenetration without altering the network topology upon guest inclusion indicates that the grid networks have a strong preference for the aromatic guests over the polar molecules like MeOH and $CHCl_3$. If only the polar MeOH and $CHCl_3$ solvent molecules are present in the reaction system, the spacious grid networks prefer to interpenetrate to eliminate cavity, but when aromatic molecules are introduced into the reaction system, the networks prefer to accommodate the guests by reducing the interpenetration. Such aromatic guest favor may be due to formation of the hydrophobic void space surrounded by phenyl and methyl groups of ImBNN.

In general, the doubly interpenetrated frameworks maintain the comparable cavity size and potential solvent-accessible areas with respect to different sizes of the guest molecules (see Table 2). This is due to the fact that the accommodation of the guests of varied sizes is adjusted by guest numbers (two or one) other than a significant change of the grid frameworks themselves (Figure 6). However, in order to clathrate guest molecules, the grid networks do exhibit flexibility to adjust the grid shape to match the guests. As seen from Table 2, the grids in Cd(II) complexes **3**−**6** have sizes of ca. 37.5 × 20.2 Å and vertex angles of ca. 123 and 57°, and those in Mn(II) complexes **7**−**11** have almost the same sizes and vertex angles. Compared to those of guest-free networks in **1** and **2**, the grids are elongated in one diagonal direction and compressed in another diagonal direction. Thus, the 2-fold interpenetrated networks show contracting/expanding structural transformation in comparison to the 3-fold interpenetrating networks upon the guest molecules' accommodation. When the size of guest molecule is increased, the long M···M separation of the grid turns slightly longer, while the short M···M separation of the grid turns slightly shorter. In addition, the crystal system turns to lower symmetry when bigger guests are introduced, changing from orthorhombic to monoclinic groups (Table 3). These observations indicate that the current grid networks feature tunable interpenetration and potential flexibility responsive to the guests' inclusion.[10,11]

Guest Removal Behavior. The thermostability and guest desorption behavior of all complexes were studied by thermogravimetric analyses (TGA), as depicted in Figure 7 and Figures S5 and S6 (Supporting Information). The guest-free complexes **1** and **2** show no obvious weight loss up to 350 °C. The TG curve of **3** shows a weight loss of 9.8% in the temperature range from 35 to 275 °C, corresponding to the loss of one *o*-xylene molecule (calculated 8.5%). The framework may be anticipated to collapse from 360 to 680 °C, as seen from Figure 7. Other Cd(II) complexes, **4**−**6**, show a similar framework decomposition process (Figure S5, Supporting Information), remaining undecomposed up to about 350 °C. All of the guest molecules hosted inside the framework voids could be released by heating. The guest release procedure may be related to the volatility of guest molecules. For a comparison, the guest-included framework containing pyrene (**6**) loses pyrene molecules in a narrow temperature range of 250−290 °C, while the temperature for the loss of *o*-xylene in framework **3** falls within a relatively long range. The TGA results for the Mn(II) coordination polymers of **7**−**10** also suggest that the guest molecules hosted inside the framework voids could escape upon heating, showing similar weight loss patterns to those of the Cd(II) analogues in the temperature range 350−700 °C. The Mn(II) frameworks remain undecomposed up to about 370 °C, slightly more stable than the Cd(II) analogues. It is also noticeable that some complexes are efflorescent, behaving in TG curves as a long, gradual guest-loss procedure even at low temperatures (below 100 °C), such as, for example, both the Cd(II)/Mn(II) complexes containing naphthalene guests. Due to the volatility of naphthalene, the guest molecules escape over a prolonged time, and the guest contents are thus not consistent between elemental analysis, X-ray single-crystal diffraction, and TGA. This implies that the guest molecules may not be uniformly spread in the cavities in the bulk samples, and escape of the guests from the crystal lattice is inherently associated with the nature of the guest molecules.

In particular, the guest-desorption behavior of complex **5** was investigated by both TG and X-ray power diffraction analyses, as shown in Figures 8 and 9, respectively. The TG curve of the fresh sample of **5** shows a weight loss of 7.7% in the temperature range 30−300 °C, corresponding to the loss of half of a phenanthrene molecule (calculated 7.2%), which is consistent with the single-crystal analysis result. The coordination framework collapses immediately after removal of the guest molecules in the range 350−650 °C (Figure 8). The guest-free sample $\{Cd(ImBNN)_2(CF_3SO_3)_2\}_n$ was obtained by heating the as-prepared sample of **5** to 280 °C for 5 days in vacuum. The TG analysis of the guest-removed sample shows no weight loss before 350 °C, confirming that all guest molecules had been evacuated. The solid-state phase information before and after desorption of the guest molecules has been checked by XRD measurements. The as-prepared sample exhibits an XRD pattern that closely matches the simulated one on the basis of the single-crystal analysis (Figure 8a and b). However, the XRD pattern of the guest-removed complex is remarkably different from the guest-included one (Figure 8c), suggesting the occurrence of structural transformation upon guest removal. Unfortunately, the single-crystallinity of the sample cannot be retained after evacuation of the guest molecules upon heating;

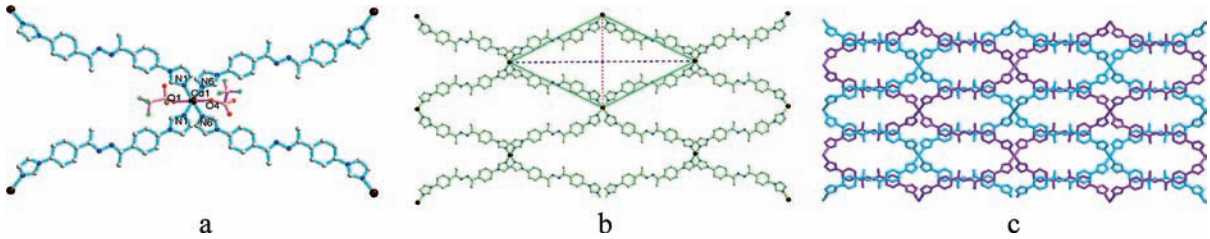

Figure 4. Representative crystal structures of the 2-fold interpenetrated networks in **3**−**11**: (a) molecular structure showing coordination geometry of metal ion, (b) (4, 4) network showing grid size, and (c) 2-fold interpenetration of the grid networks. The guest molecules and anions are omitted.

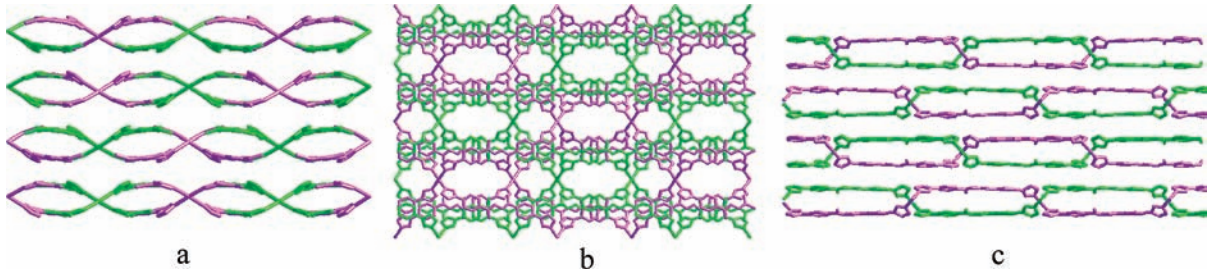

Figure 5. Crystal packing of the doubly interpenetrating networks: (a) viewed along the *a* axis in **3** and the *b* axis in **7**, (b) viewed along the *b* axis in **3** and the *a* axis in **7**, and (c) viewed along the *c* axis in **3** and **7**. The guest molecules and anions are omitted.

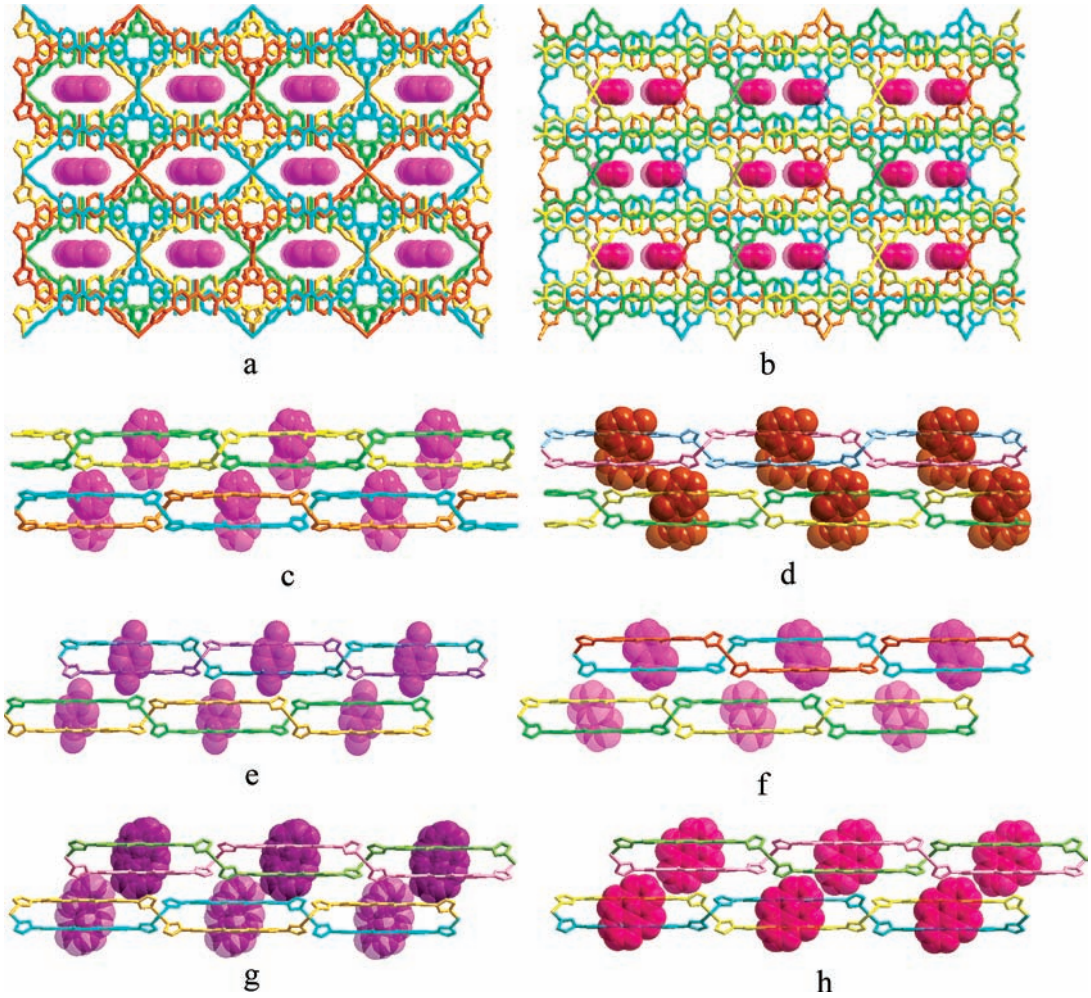

Figure 6. Guest filled crystal packing of the 2-fold interpenetrating networks with guest molecules shown in the space-fill model (a) for guest molecules viewed along the *a* axis in **4**−**6** and **8**−**11**, (b) for benzene guests viewed along the *b* axis in **7**, (c) for benzene guests viewed along the *c* axis in **7**, (d) for *o*-xylene guests viewed along the *c* axis in **3**, (e) for *p*-xylene guests viewed along the *b* axis in **8**, (f) for naphthalene guests viewed along the *b* axis in **4** and **9**, (g) for phenanthrene guests viewed along the *b* axis in **5** and **10**, and (h) for pyrene guests viewed along the *b* axis in **6** and **11**. The anions are omitted for clarity.

therefore, the detailed structural change is not clear at present. These results show that the 2-fold interpenetrating Cd(II)/Mn(II) grid coordination polymers contain cavities capable of hosting various aromatic guests. Removal of the guest

Table 3. The Crystal Data and Structure Refinement Summary for **1**−**11**

	1	**2**	**3**	**4**	**5**	**6**
empirical formula	$C_{46}H_{40}CdF_6N_{12}O_6S_2$	$C_{46}H_{39}F_6MnN_{12}O_6S_2$	$C_{54}H_{48}CdF_6N_{12}O_6S_2$	$C_{51}H_{44}CdF_6N_{12}O_6S_2$	$C_{53}H_{45}CdF_6N_{12}O_6S_2$	$C_{54}H_{45}CdF_6N_{12}O_6S_2$
fw	1147.42	1088.95	1251.56	1211.50	1236.53	1248.54
space group	*Pc*2(1)*b*	*Pca*2(1)	*Pbcm*	*C*2/*m*	*C*2/*m*	*C*2/*m*
a/Å	11.8256(3)	23.823	18.8212(3)	19.5599(8)	19.8238(13)	19.8224(9)
b/Å	17.5321(5)	11.723	14.3326(4)	20.1708(6)	20.2114(7)	20.2471(7)
c/Å	23.7164(7)	17.431	20.2184(4)	15.0295(6)	15.1437(8)	15.0929(6)
α/deg	90.00	90.00	90.00	90.00	90.00	90.00
β/deg	90.00	90.00	90.00	115.821(4)	117.056(6)	116.040(4)
γ/deg	90.00	90.00	90.00	90.00	90.00	90.00
V/Å^3	4917.1(2)	4868.0	5454.0(2)	5337.7(3)	5403.6(5)	5442.6(4)
Z	4	4	4	4	4	4
ρ_{calcd} /g cm^{-3}	1.550	1.486	1.524	1.508	1.520	1.524
μ/mm^{-1}	0.0613	0.442	0.560	0.569	0.564	0.561
T/K	150(2)	150(2)	153(2)	153(2)	153(2)	153(2)
R_{int}	0.0592	0.0287	0.0593	0.0266	0.0341	0.0308
R_1	0.0510	0.0423	0.1031	0.0398	0.0333	0.0325
wR_2	0.0961	0.1047	0.2422	0.1112	0.0823	0.0906

	7	**8**	**9**	**10**	**11**
empirical formula	$C_{52}H_{46}F_6MnN_{12}O_6S_2$	$C_{50}H_{45}F_6MnN_{12}O_6S_2$	$C_{51}H_{44}F_6MnN_{12}O_6S_2$	$C_{53}H_{45}F_6MnN_{12}O_6S_2$	$C_{54}H_{45}F_6MnN_{12}O_6S_2$
fw	1168.07	1143.02	1154.04	1179.07	1191.08
cryst syst	orthorhombic	monoclinic	monoclinic	monoclinic	monoclinic
space group	*Pca*2(1)	*C*2/*m*	*C*2/*m*	*C*2/*m*	*C*2/*m*
a/Å	14.1224(6)	19.9472(8)	19.5803(11)	19.8238(13)	19.6416(8)
b/Å	18.5037(11)	20.2514(6)	20.3044(10)	20.2114(7)	20.2360(6)
c/Å	20.4473(9)	14.8379(5)	14.9232(7)	15.1437(8)	15.0415(5)
α/deg	90	90	90	90.00	90.00
β/deg	90	117.331(4)	116.507(5)	117.056(6)	116.391(4)
γ/deg	90	90	90	90.00	90.00
V/Å^3	5343.2(5)	5324.8(3)	5309.3(5)	5403.6(5)	5355.4(3)
Z	4	4	4	2	4
ρ_{calcd} /g cm^{-3}	1.452	1.423	1.444	1.449	1.477
μ/mm^{-1}	0.408	0.408	0.410	0.404	0.409
T/K	153(2)	153(2)	153(2)	153(2)	153(2)
R_{int}	0.0559	0.0376	0.0476	0.0427	0.0273
R_1	0.626	0.0639	0.0494	0.0423	0.0569
wR_2	0.1923	0.1718	0.1035	0.0750	0.1596

molecules is possible by heating the guest inclusion products. However, structural transformation may occur after release of the guests, although the TG analyses indicate apparent high thermostability (above 300 °C).

Further experiments have been carried out to explore the possibility of guest exchange and selectivity toward different guest molecules. It was found that, if a mixture of aromatic molecules of different sizes was introduced in the reaction system, the bigger-sized guest was preferentially selected to crystallize. However, when the guest-included Cd(II)/Mn(II) complexes were put in a solution containing other guest molecules, no guest exchange could be observed. This may suggest that such frameworks show no unique selectivity toward the size and shape of different aromatic guests. The rigidity of the ImBNN ligand endows the formation of large cavities inside the framework and inclusion of various aromatic guests, on one hand, and is too rigid to allow further guest exchange and specific guest size selectivity, on the other hand.

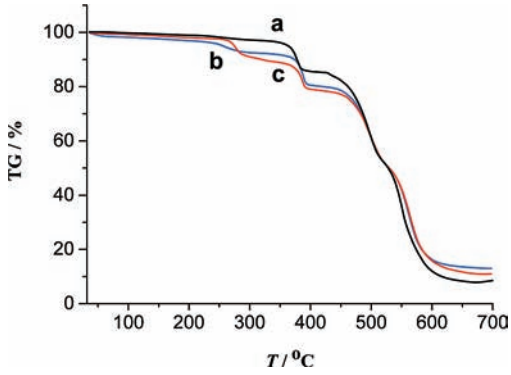

Figure 7. TG curves for complexes (a) **2**, (b) **3**, and (c) **6**.

Conclusions

On the basis of a long rigid N,N′-type ligand, ImBNN, a series of Cd(II)/Mn(II) rhombic-grid coordination polymers has been synthesized with $CF_3SO_3^-$ as counteranions. Guest-free structures were obtained as triply interpenetrated coordination networks, while inclusion of the aromatic guest

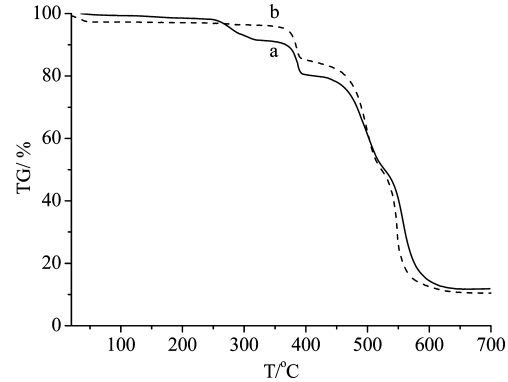

Figure 8. TG curves for complex **5**: (a) as-prepared sample and (b) after the guests were removed.

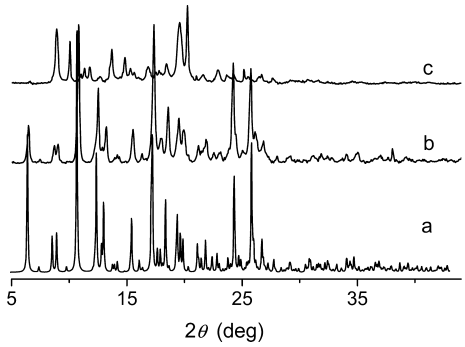

Figure 9. X-ray powder diffraction patterns of complex **5**: (a) simulated, (b) measured from as-prepared sample, and (c) after removing the guest molecules.

molecules led to a change of the triply interpenetrated networks to doubly interpenetrated ones accompanied by grids of contracting/expanding change. The resulting 2-fold entangled networks contain cavities displaying a strong preference and remarkable tolerance toward various aromatic guests, such as benzene, *o*-/*p*-xylenes, naphthalene, phenanthrene, and pyrene. However, no unique selectivity among these aromatic molecules of varied sizes could be observed through guest exchange tests, although the bigger guest molecules are obviously preferred during network assembly and crystallization. The guest molecules are removable by heating the guest-included frameworks, when the structural transformation may occur. In general, the coordination networks assembled in this work feature (a) a ready formation of grid networks under conditions with or without guest molecules, (b) interpenetration adjustable through the inclusion of guest molecules, (c) framework flexibility responsive to guest molecules, and (d) structure change upon the inclusion/removal of guest molecules. These advantages make it possible to find an approach for the synthesis of flexible coordination polymers along this line,[15] which represents a promising field pointing toward smart materials that can sense, process, or actuate a response to external stimuli.[16]

Experimental Section

All starting materials and solvents were obtained from commercial sources and used without further purification. The ligand ImBNN was synthesized following the literature methods.[14] Infrared spectra were measured on a Nicolet/Nexus-670 FT-IR spectrometer with KBr pellets. The X-ray powder diffraction was recorded on a Brucker D8 Advance diffractometer at 40 kV and 40 mA with a Cu-target tube and a graphite monochromator. TGA was performed in the air and under 1 atm of pressure at a heating rate of 10 °C/min on a NETZSCH Thermo Microbalance TG 209 F3 Tarsus apparatus.

$[Cd(ImBNN)_2(CF_3SO_3)_2]_n$ (1). $Cd(CF_3SO_3)_2 \cdot 6H_2O$ (0.026 g, 0.05 mmol) was dissolved in methanol (3 mL) and then carefully layered onto a solution of ImBNN (0.019 g, 0.05 mmol) in $CHCl_3$ (3 mL). After about a week, yellow block crystals suitable for single-crystal X-ray diffraction analysis formed at the interface of the two solutions. Yield: 10 mg, 35%. Elem anal. calcd for $CdC_{46}H_{45}N_{12}O_{8.5}S_2F_6$ (**1**·$2.5H_2O$, 1192.46): C, 46.33; H, 3.80; N, 14.10. Found: C, 46.77; H, 3.89; N, 13.74%. IR (cm^{-1}, KBr): 3124m, 1608m, 1575w, 1522s, 1494m, 1425m, 1301s, 1258s, 1236s, 1167s, 1122m, 1061s, 1030s, 964m, 932w, 838m, 758m, 655m, 637s, 568m, 519m.

$[Mn(ImBNN)_2(CF_3SO_3)_2]_n$ (2). $Mn(CF_3SO_3)_2$ (0.018 g, 0.05 mmol) was dissolved in methanol (3 mL) and then mixed with a solution of ImBNN (0.019 g, 0.05 mmol) in $CHCl_3$ (3 mL). The mixed solution was diffused by Et_2O vapor. After about 2 days, yellow block crystals suitable for single-crystal X-ray diffraction analysis formed. Yield: 11 mg, 40%. IR (cm^{-1}, KBr): 3126m, 2960w, 1607s, 1522s, 1427m, 1368m, 1305s, 1236s, 1166s, 1118sm, 1062s, 1029s, 963m, 931m, 838s, 748m, 657m, 635s, 567m, 514m.

$\{[Cd(ImBNN)_2(CF_3SO_3)_2]\supset C_8H_{10}\}_n$(3). $Cd(CF_3SO_3)_2 \cdot 6H_2O$ (0.026 g, 0.05 mmol) was dissolved in methanol (3 mL) and then carefully layered onto a solution of ImBNN (0.019 g, 0.05 mmol) in $CHCl_3$/*o*-xylene (4 mL/3 mL). After about a week, yellow block crystals suitable for single-crystal X-ray analysis formed at the interface of the two solutions. Yield: 12 mg, 42%. Elem anal. calcd for $CdC_{54}H_{52}N_{12}O_7S_2F_6$, (**3**·$H_2O$, 1271.60): C, 51.00; H, 4.12; N, 13.22. Found: C, 50.83; H, 3.929; N, 13.28%. IR: (cm^{-1}, KBr): 3457m, 3121m, 1713w, 1604s, 1521s, 1426w, 1367m, 1297s, 1251s, 1169s, 1063s, 1027s, 963m, 931m, 835s, 737m, 636s, 571m, 514m.

$\{[Cd(ImBNN)_2(CF_3SO_3)_2]\supset(C_{10}H_8)_{1/2}\}_n$(4). $Cd(CF_3SO_3)_2 \cdot 6H_2O$ (0.026 g, 0.05 mmol) was dissolved in methanol (3 mL) and carefully layered on a mixture solution of naphthalene-saturated methanol solvent (2 mL) and ImBNN (0.019 g, 0.05 mmol) dissolved in $CHCl_3$ (4 mL). After about a week, yellow block crystals suitable for single-crystal X-ray analysis formed at the interface of the two solutions. Yield (based on ligand): 14 mg, 46%. IR: (cm^{-1}, KBr): 3122m, 2923w, 1604m, 1521s, 1422m, 1366m, 1297s, 1258s, 1238s, 1173m, 1121m, 1061s, 964m, 932w, 842m, 795w, 757w, 654m, 636s, 570m, 513m, 482w.

$\{[Cd(ImBNN)_2(CF_3SO_3)_2]\supset(C_{14}H_{10})_{1/2}\}_n$(5). $Cd(CF_3SO_3)_2 \cdot 6H_2O$ (0.026 g, 0.05 mmol) was dissolved in methanol (3 mL) and carefully layered on a mixture solution of phenanthrene (15 mg) and ImBNN (0.019 g, 0.05 mmol) dissolved in $CHCl_3$ (6 mL). After about a week, yellow block crystals suitable for single-crystal X-ray analysis formed at the interface of the two solutions. Yield (based on ligand): 13 mg, 42%. Elem anal. calcd for $CdC_{53}H_{45}N_{12}O_6S_2F_6$ (1236.53): C, 51.48; H, 3.67; N, 13.59. Found: C, 51.05, H, 3.74; N, 13.45%. IR (cm^{-1}, KBr): 3123m, 2922w, 1605m, 1576m, 1521s, 1493w, 1424m, 1365m, 1298s, 1259s, 1237s, 1172m, 1120m, 1061s, 1031s, 964m, 932w, 834m, 742m, 639s, 636s, 569m, 516m, 482w.

$\{[Cd(ImBNN)_2(CF_3SO_3)_2]\supset(C_{16}H_{10})_{1/2}\}_n$ (6). $Cd(CF_3SO_3)_2 \cdot 6H_2O$ (0.026 g, 0.05 mmol) was dissolved in methanol (3 mL) and carefully layered on a mixture solution of pyrene (20 mg) and ImBNN (0.019 g, 0.05 mmol) dissolved in $CHCl_3$ (6 mL). After about a week, yellow block crystals suitable for single-crystal X-ray analysis formed at the interface of the two solutions. Yield: 14 mg, 45%. Elem anal. calcd for $([Cd(ImBNN)_2(CF_3SO_3)_2]\cdot(C_{16}H_{10})_{2/3}$, 1282.93): C, 53.10; H, 3.67; N, 13.10. Found: C, 53.03; H, 3.83; N, 13.59%. IR (cm^{-1}, KBr): 3123m, 1604m, 1574w, 1520s, 1421w, 1364m, 1293s, 1254s, 1235s, 1176s, 1120m, 1063s, 1029s, 964m, 932w, 842s, 759m, 736w, 716w, 657m, 636s, 570m, 515m.

$\{[Mn(ImBNN)_2(CF_3SO_3)_2]\supset(C_6H_6)\}_n$(7). $Mn(CF_3SO_3)_2$ (0.018 g, 0.05 mmol) was dissolved in methanol (3 mL) and then mixed with a solution of ImBNN (0.019 g, 0.05 mmol) in $CHCl_3$/benzene (1:1; 6 mL). The mixed solution was diffused by Et_2O vapor. After about 2 days, yellow block crystals suitable for single-crystal X-ray diffraction analysis formed. Yield: 13 mg, 45% (based on ligand).

(15) (a) Fletcher, A. J.; Thomas, K. M.; Rosseinsky, M. J. *J. Solid. State Chem.* **2005**, *178*, 2491–2510. (b) Kitagawa, S.; Uemura, K. *Chem. Soc. Rev.* **2005**, *34*, 109–119.

IR (cm^{-1}, KBr): 3126m, 1663w, 1060s, 1522s, 1496m, 1425w, 1366m, 1303s, 1057s, 1170s, 1120w, 1061s, 1030s, 964m, 932w, 837s, 761w, 685w, 657m, 637s, 570m, 515m.

{[Mn(ImBNN)$_2$(CF$_3$SO$_3$)$_2$]⊃(C$_8$H$_{10}$)$_{1/2}$}$_n$(8). This complex was prepared using a procedure analogous to that described for **7**, replacing benzene with *p*-xylene, yielding the desired product (42%). IR (cm^{-1}, KBr): 3126m, 1606m, 1521s, 1303w, 1238s, 1174m, 1116w, 1064s, 1029s, 964m, 931m, 842m, 756w, 670m, 636s, 570m, 514w.

{[Mn(ImBNN)$_2$(CF$_3$SO$_3$)$_2$]⊃(C$_{10}$H$_8$)$_{1/2}$}$_n$(9). Mn(CF$_3$SO$_3$)$_2$ (0.018 g, 0.05 mmol) was dissolved in methanol (3 mL) and then added into a mixed solution of MeOH (3 mL) saturated by naphthalene and ImBNN (0.019 g, 0.05 mmol) in $CHCl_3$ (3 mL). The mixture was diffused by Et_2O vapor. After about 4 days, yellow block crystals suitable for single-crystal X-ray diffraction analysis formed. Yield: 12 mg, 42% (based on ligand). IR (cm^{-1}, KBr): 3126m, 1606m, 1522s, 1424w, 1366m, 1302s, 1258s, 1175m, 1119w, 1061s, 1030s, 964m, 932w, 842m, 793w, 758w, 658w, 637m, 570m, 515w.

{[Mn(ImBNN)$_2$(CF$_3$SO$_3$)$_2$]⊃(C$_{14}$H$_{10}$)$_{1/2}$}$_n$(10). Mn(CF$_3$SO$_3$)$_2$ (0.018 g, 0.05 mmol) was dissolved in methanol (3 mL) and then added into a solution of phenanthrene (20 mg) and ImBNN (0.019 g, 0.05 mmol) in $CHCl_3$ (6 mL). The mixture was diffused by Et_2O vapor. After about 3 days, yellow block crystals suitable for single-crystal X-ray diffraction analysis formed. Yield: 12 mg, 40% (based on ligand). IR (cm^{-1}, KBr): 3125m, 1606m, 1574w, 1521s, 1424w, 1365m, 1304s, 1235s, 1176m, 1118w, 1062m, 1029s, 964m, 931w, 833m, 743w, 659w, 636m, 569m.

{[Mn(ImBNN)$_2$(CF$_3$SO$_3$)$_2$]⊃(C$_{16}$H$_{10}$)$_{1/2}$}$_n$ (11). This complex was prepared using a procedure analogous to that described for **10**, replacing phenanthrene with pyrene, yielding the desired product (35%). IR (cm^{-1}, KBr): 3130m, 1607m, 1521s, 1366m, 1300s, 1259s, 1168m, 1115w, 1063m, 1032s, 966m, 837m, 755w, 637w, 572m, 515w.

X-Ray Structure Analyses. The intensity data of all complexes were collected on an Oxford Gemini S Ultra diffractometer equipped with graphite monochromated Enhance (Mo) X-ray source ($\lambda = 0.71073$ Å). The structures were solved by the direct methods following difference Fourier syntheses and refined by the full-matrix least-squares method against F_o^2 using the SHELXTL software.[17] Except those displaying severe disorder, the non-hydrogen atoms were refined anisotropically, while hydrogen atoms were introduced in calculated positions. In complexes **3**−**6** and **8**−**11**, the $CF_3SO_3^-$ anions show crystallographically imposed disorder at two adjacent positions. The solvated phenanthrene molecules in complexes **5** and **10** are distributed over two sites, which were assigned fractional occupancy with a sum equal to 1. Complex **7** is a racemic twinning structure showing pseudosymmetry to *Pbcm*. However, the refinement in this space group gave rise to a high R1 value of 0.1568. Therefore, the space group *Pca*(21) was assigned, which gave satisfactory refinement, with the R1 value being 0.0626. The benzene molecules are disordered over two positions and refined fractionally. In case of disorder, appropriate restraints were applied to model the molecules to the idealized geometry. Crystallographic data for complexes **1**−**11** are summarized in Table 3. Selected bond lengths and bond angles are listed in Tables S1−S3 (Supporting Information). CCDC 698700−698710 contain the supplementary crystallographic data for this paper. These data can be obtained free of charge from The Cambridge Crystallographic Data Centre via www.ccdc.cam.ac.uk/data_request/cif.

Acknowledgment. This work was supported by the NSF for Distinguished Young Scholars of China (Grant 20525310), 973 Program of China (Grant 2007CB815302), the NSF of China (Grants 20673147, 20773167, 20731005) and RFDP of Higher Education.

Supporting Information Available: X-ray crystallographic data (CIF format), selected bond lengths and bond angles, additional crystal structure figures, XRD patterns and TGA curves. This material is available free of charge via the Internet at http://pubs.acs.org.

IC801770N

(16) Wang Z. L.; Kang, Z. C. *Functional and Smart Materials: Structural Evolution and Structure Analysis*; Plenum Press: New York, 1998.
(17) Sheldrick, G. M. *SHELX-97*; University of Götingen: Götingen, Germany, 1997.